TERAHERTZ BWO-SPECTROSOPY

B. Gorshunov,[1] A. Volkov,[1] I. Spektor,[1] A. Prokhorov,[1] A. Mukhin,[1] M. Dressel,[2] S. Uchida,[3] and A. Loidl[4]

[1]*A.M. Prokhorov General Physics Institute, Russian Academy of Sciences*
Moscow, Russia
[2]*1. Physikalisches Institut, Universität Stuttgart*
Stuttgart, Germany
[3]*University of Tokyo*
Tokyo, Japan
[4]*Institute of Physics, University of Augsburg*
Augsburg, Germany

Abstract

Modern Terahertz-subTerahertz (THz-subTHz) spectrometers, based on continuously frequency-tunable coherent sources of radiation, the backward-wave oscillators (BWOs), are described which cover the frequencies ν = 1 cm^{-1} – 50 cm^{-1} (0.03 – 1.5 THz) and allow for measurements at temperatures 2 – 1000 K, also in magnetic fields. They allow for direct determination of spectra of any optical parameter of a material at millimeter-submillimeter wavelengths, the domain where infrared or microwave spectrometers encounter serious methodological difficulties. We report on new technical abilities of the quasioptical BWO-spectrometers and discuss their main components. We demonstrate abilities of the THz-subTHz BWO-spectroscopy by presenting some latest results on measurements of dielectric, conducting, superconducting and magnetic materials.

1. Introduction

More than 20 years ago a way of mastering the millimeter-submillimeter (mm-submm) wavelength or subTeragertz - Terahertz frequency ranges for spectroscopic purposes was outlined, based on coherent, continuously frequency-tunable radiation sources, backward-wave oscillators, and on a quasioptical manner of handling the radiation in measurement schemes (a review is given in [1]). Modern generation of BWO-based frequency-domain spectrometers allow for any sort of spectroscopic characterization of solid,

liquid or gaseous samples, they have made it possible to close the so-called "spectroscopic gap" or the "Terahertz gap" on the electromagnetic scale – frequencies 10^{11} Hz < ν < 10^{12} Hz (Fig.1).

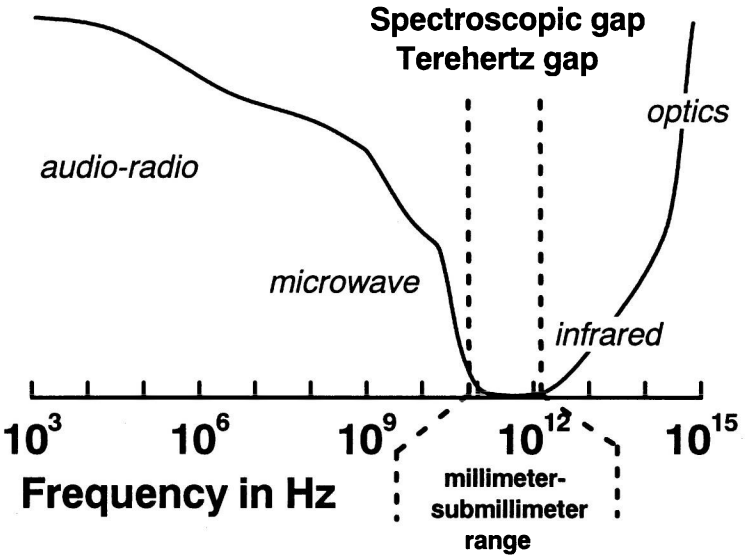

Fig.1. Schematically and qualitatively: availability of different spectral ranges for spectroscopic measurements. The millimeter-submillimeter range is indicated as a "spectroscopic gap".

The THz-subTHz BWO-spectrometers are of a hybrid type and combine merits of techniques of neighboring wavelength domains – microwave and infrared: "high quality" of the working radiation (highly monochromatic, powerful, spectrally bright and polarized, finely frequency-tunable), on one hand, and the broad-band flexible quasioptical measurement schemes (no waveguides are used, radiation is travelling in free space), on the other hand.

The main feature important for spectroscopists is that the spectrometers allow for a *direct* determination of the *polarized spectra* of any optical quantity of the material under study: real and imaginary parts of refractive index $n^*(\nu) = n(\nu) + ik(\nu)$, dielectric constant $e^*(\nu) = e'(\nu) + ie''(\nu)$, dynamical conductivity $s^*(\nu) = s'(\nu) + is''(\nu)$, magnetic permeability $\mu^*(\nu) = \mu'(\nu) + i\,\mu''(\nu)$, etc.

"Direct" means that no additional manipulations are needed, like the Kramers-Kronig analysis. Measurements can be performed at frequencies ν = 0.03 – 1.5 THz and temperatures 2 – 1000 K, under external magnetic fields when needed (in the Oxford cryostat Spectromag, up to 8 Tesla). Measurements with linear, circular or elliptic polarizations are possible.

In this paper we describe main principles of the THz BWO-based quasioptical spectrometers and present some typical results demonstrating their ability to measure electrodynamical parameters of various substances.

2. Spectroscopic principle

The spectroscopic principle employed in the BWO-spectroscopy is as follows. Since any dielectric material is characterized by two optical parameters (we do not consider magnetic materials for a moment, assuming $\mu'=1$ and $\mu''=0$), the spectra of *two* quantities are measured experimentally: the transmission coefficient $Tr_{exp.}(\nu)$ of a plane-parallel sample and the phase shift $f_{exp.}(\nu)$ of the radiation passed through this sample. Then the two unknowns, say, ε' and ε'', are directly calculated using Fresnel expressions for a complex transmissivity of a plane-parallel slab (ex. [2]), by solving the set of two corresponding equations for various frequencies:

$$\left.\begin{aligned} Tr(\varepsilon', \varepsilon'', \nu) &= Tr_{exp.}(\nu) \\ f(\varepsilon', \varepsilon'', \nu) &= f_{exp.}(\nu) \end{aligned}\right\}$$

This is demonstrated in Fig.2, which also shows that any other optical quantity can be calculated basing on ε' and ε'', according to the well-known expressions [2].

We note that the sample can be also in the form of one or two thin films (dielectric, conducting, superconducting) grown on one or both sides of a dielectric substrate. In this case, after the dielectric properties of the substrate have been measured beforehand, the parameters of the film are determined in the same way, using now the $Tr(\varepsilon',\varepsilon'')$ and $f(\varepsilon',\varepsilon'')$ Fresnel expressions for a *two-* or *three-layered* system, respectively [2]. This is demonstrated in Figs.3,4, where the spectra of transmission and phase shift of corresponding two- or three layered system are shown: superconducting NbN films on a sapphire substrate. From theses figures it is also seen that the accuracy of the film conductivity measurement in the superconducting state is increased significantly when two films on the substrate are measured.

The BWO-spectrometers allow also to measure the dielectric properties of liquid samples. For that a cuvette can be made of two plane-parallel "windows" with the liquid placed in-between; the windows have to be made of a material which is transparent for the THz radiation. Having the dielectric properties of the "windows" measured beforehand, the transmission and the

phase shift of this sort of 3-layered system are measured and then with an appropriate software the parameters of the liquid under study are determined. A convenient way of measuring liquids is provided by the "tester" technique [3]. In the experiment, the reflectivity spectrum is recorded of a "tester" – a plane-parallel transparent

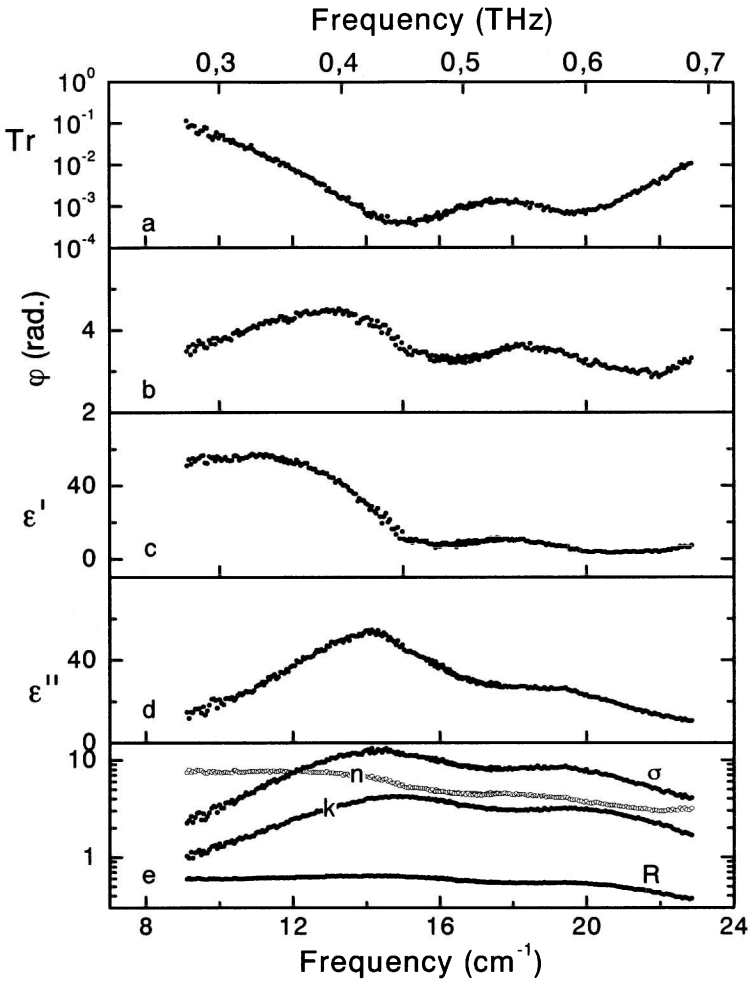

Fig.2. Spectra of transmission coefficient Tr (a) and phase shift φ (b) of a plane-parallel sample $TlGaSe_2$ (thickness 0.1 mm). Panels c, d, e show the spectra of

optical parameters calculated on the basis of Tr and φ spectra: real ε′ and imaginary ε″ parts of dielectric constant, conductivity σ (in $Ohm^{-1}cm^{-1}$), reflection coefficient R, calculated on the basis of ε′(ν) and ε″(ν) spectra.

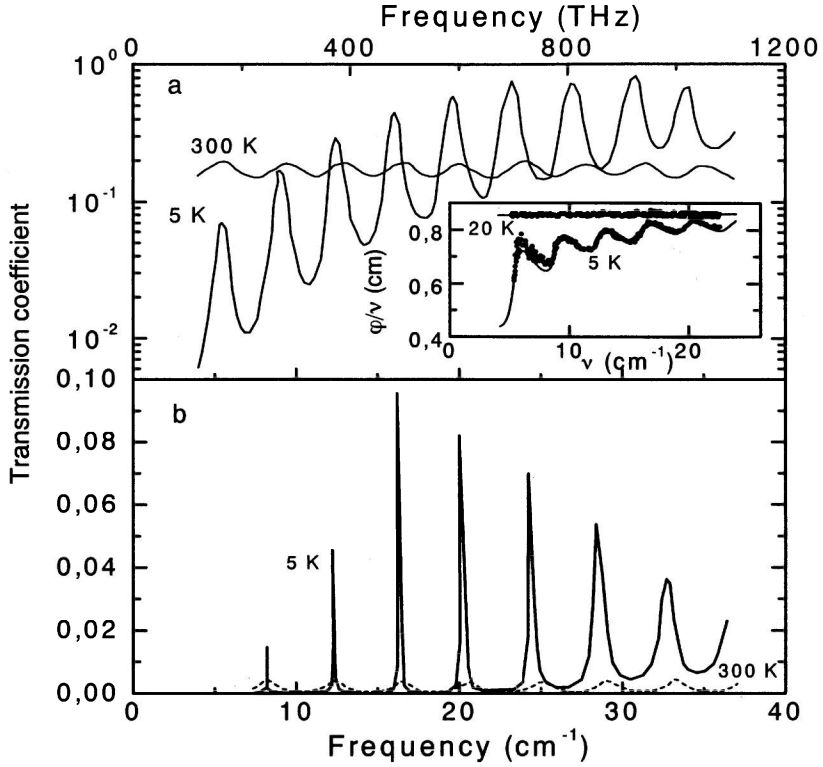

Fig.3. Spectra of transmission coefficient and phase shift of thin NbN superconducting film on sapphire substrate at two temperatures, above and below the superconducting transition temperature. Panel (a) corresponds to a single film on a substrate and panel (b) - to two films on a substrate. Dots in the inset shows experiment and the line – theoretical fit.

plate with the dielectric parameters refractive index n, extinction coefficient k and measured beforehand. The spectrum contains periodic interferometric minima [2]. When a liquid sample is put on the top of the tester, the elctrodynamic properties of the interface "tester-liquid" change and this leads to the frequency shift of every interferometric minima and to the change of its

amlitude (depth). Measurement of these two changes in the experiment allows to calculate two unknown dielectric parameters of the liquid under study, as demonstrated in Fig.5.

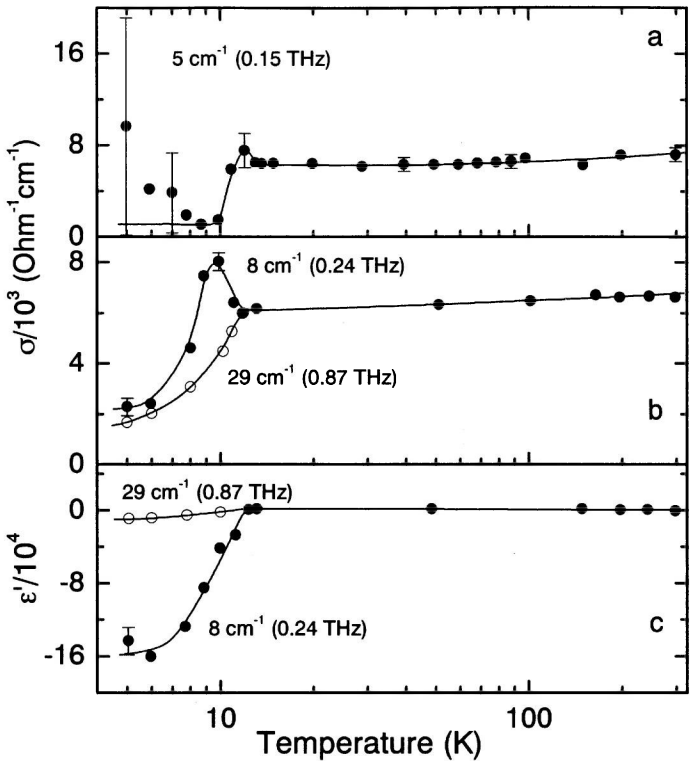

Fig.4. Temperature dependences of dynamical conductivity and dielectric constant of NbN superconducting films on sapphire substrate at two frequencies, in normal and superconducting states. Panel (a) shows the result of measurement of a single film on a substrate, when the accuracy is low in the superconducting state. It is strongly enhanced for a measurement configuration when two films are deposited on a substrate, panel (b). Lines re guides to the eye.

For the magnetically active materials having $\mu' \neq 1$ and $\mu'' \neq 0$, there are, in general, *four* optical parameters to be determined, ε', ε'', μ' and μ''. In such a case to determine all of them, one has to measure *also four* experimental quantities. These can be Tr, f, reflection coefficient R and the reflection

coefficient phase ψ. The situation, however, is essentially simplified in cases when magnetic phenomena manifest themselves in the form of sharp and narrow resonances (for example, AFMR-modes in antiferromagnetic dielectrics, rear-earth modes in rear-earth dielectrics, magnetic resonance in molecular

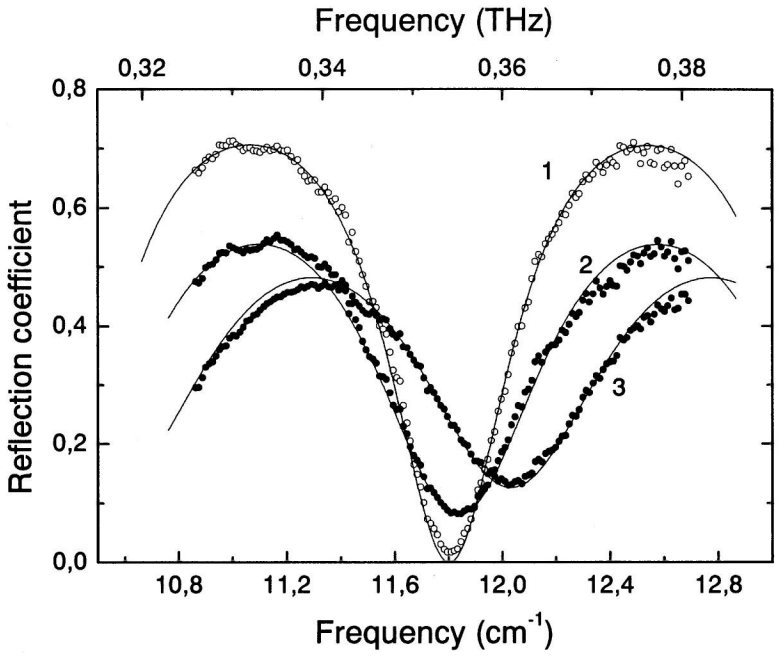

Fig.5. Spectra of reflection coefficient of a plane-parallel transparent plate made of Si (1), of Si plate with alcohol (2) and water (3) put on its "back" side. Dots – experiment, lines – fits based on Fresnel expressions [2] allowing for determination of the dielectric parameters of liquids, see text.

magnets). Then the real part of the magnetic susceptibility μ′ is very close to unity and the imaginary part of it μ″ – to zero at all frequencies except this resonance vicinity. In such situation one can "separate" the dielectric and the magnetic measurements by measuring, firstly, the dielectric parameters ε′ and ε″ *outside* the magnetic dispersion range employing the standard method and then interpolating the so-obtained ε′ and ε″ into the "magnetic domain" of frequencies, and assigning all changes happening in the $Tr_{exp.}(\nu)$ and $\varphi_{exp.}(\nu)$

spectra exclusively to the dispersion of μ' and μ'', which are then calculated by solving the set of two equations for $Tr(\varepsilon',\varepsilon'',\mu',\mu'')$ and $\varphi(\varepsilon',\varepsilon'',\mu',\mu'')$ [2].
We note that since all measurements on the BWO-spectrometers are done in a quasioptical arrangement, the sample under study has to be of transverse size d larger than the wavelength in the sample λ/n, typically, $d = 3\lambda/n$ [1], to avoid undesirable diffraction effects. It should be noted, however, that the latest achievements made it possible to adopt the near-field spectroscopic ideas
to the BWO-based quasioptics and thus to investigate samples with sizes much smaller than λ [4].

Below we briefly describe basic measurements configurations and present main characteristics of modern BWO-spectrometers.

3. Quasioptical measurement configurations

Basic configurations of quasioptical THz-subTHz measurements are presented in Fig.6. The transmission coefficient is measured in a simplest way (Fig.6a): the radiation comes through the sample and the value of the $Tr(\nu)$ is determined as a ratio of the intensity at the detector with the sample in the beam to that without the sample:

$$Tr(\nu) = I_{sample}(\nu) / I_{no\ sample}(\nu).$$

To measure the *phase shift* of the radiation passed through the sample with the thickness d_{sample} an interferometric scheme is used. It is based on the Mach-Zahnder interferometer (Fig.6b) equipped with the movable mirror (MM) which is controlled by a software and is always electronically tuned to the position providing minimal interferometric signal at the detector due to interference of the basic (thick line in Fig.6b) and the reference (thin line) beams in the two interferometer arms. During the measurement, the two positions X of the mirror MM are recorded, with ($X_{sample}(\nu)$) and without ($X_{no\ sample}(\nu)$) the sample in the measurement channel and the difference between these positions allows to calculate the absolute value of the phase shift:

$$\varphi(\nu) = 2*p*[X_{sample}(\nu) - X_{no\ sample}(\nu) + d_{sample}] * \nu,$$

where the quantities $X_{sample}(\nu)$, $X_{no\ sample}(\nu)$ and d_{sample} are expressed in cm, ν - in cm^{-1} and φ - in radians.

In the *reflection coefficient* measurement, the radiation passes through the beamsplitter BMS (Fig.6c), is reflected by the sample and detected by the detector. The absolute reflection coefficient is determined as a ratio of the intensity reflected from the sample to the intensity reflected from the reference mirror:

$$R(\nu) = \mathbf{I}_{\text{sample}}(\nu) / \mathbf{I}_{\text{reference mirror}}(\nu).$$

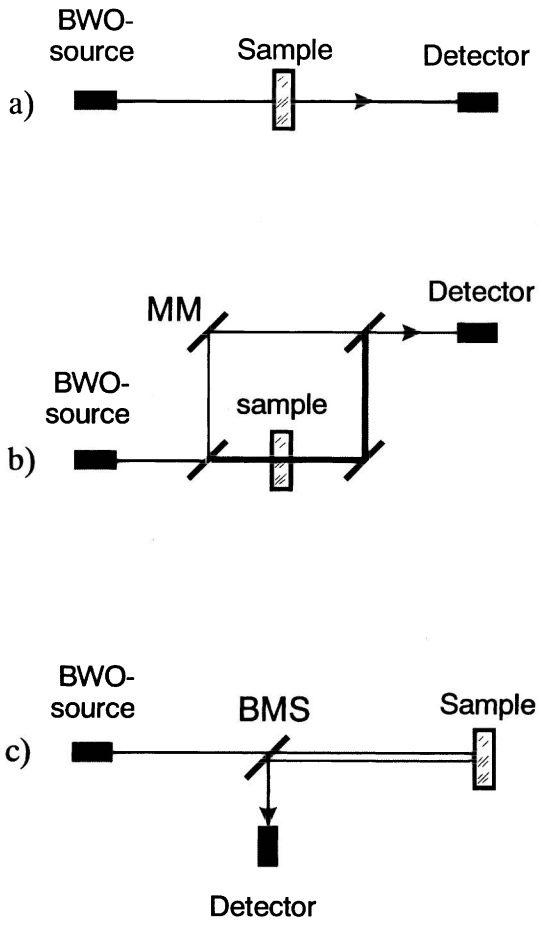

Fig.6. Schematic representation of basic measurement configurations of the quasioptical THz-subTHz BWO-spectrometer: a) geometry for measurement of transmission coefficient; b) geometry for measurement of transmitted radiation phase shift. MM is a movable mirror used for compensation of change of optical path in the Mach-Zahnder interferometer arm, introduced by a sample, c) geometry for measurement of the reflection coefficient. BMS is a semi-transparent beamsplitter (wire grid).

4. Main parameters of the BWO-spectrometer

In this paragraph the main parameters of the quasioptical BWO-spectrometer are summarized.

• Working frequency range:	
main	0.1 – 1.0 THz
extended	0.03 – 1.5 THz
• Type of measurements:	*contactless; Direct;quasioptical;*
• Measurable quantities: spectra of	
complex transmission coefficient	$Tr^*(\nu)= Tr(\nu)e^{i\varphi(\nu)}$
complex reflection coefficient	$R^*(\nu) = R(\nu)e^{i\psi(\nu)}$
complex refraction index	$n^*(\nu)= n(\nu)+ ik(\nu)$
complex dielectric function	$\varepsilon^*(\nu) = \varepsilon'(\nu) + i\varepsilon''(\nu)$
complex dynamical conductivity	$\sigma^*(\nu) = \sigma'(\nu) + i\sigma''(\nu)$
complex magnetic susceptibility	$\mu^*(\nu) = \mu'(\nu) + i\mu''(\nu)$
dielectric and magnetic loss tangent	$\varepsilon''/\varepsilon'$, μ''/μ'
absorption coefficient	$\alpha(\nu)$
birefringence	$\Delta n(\nu)$
• Frequency resolution:	
relative	$\Delta\nu/\nu \sim 10^{-4} - 10^{-5}$
average absolute	0.001 cm^{-1}.
• Dynamical range:	
main	40-45 dB
extended	45-60 dB
• Signal-to-noise ratio:	$10^4 - 10^6$
• Degree of polarization of working radiation:	99.99 %
• Time for recording the spectrum of 100 points:	
T(ν) or R(ν) spectra	10 - 20 s
φ(ν) spectrum	20 - 40 s
• Accuracy of the radiation frequency determination:	
at a separate point	better than ± 0.01%
in the working frequency interval	better than ± 0.5%
• Available temperatures:	2 - 1000 K
• Available magnetic fields:	up to 8 Tesla
• Software "Epsilon"	Windows XP, 98

All measurements and procedures of fitting and calculation of the dielectric/magnetic properties of a sample are fully PC-controlled and are conducted on a real time scale.

In the next few paragraphs we present some latest results on THz spectroscopy of materials of various kinds, from dielectric to superconducting, to demonstrate abilities of BWO-spectrometer for fundamental research.

5. THz-subTHz dielectric response of high-temperature superconductor

Fig.7 gives a demonstration of how the out-of-plane spectra of dielectric response of a high-T_c superconductor can be measured. The substance here is the Sm-based LSCO (the T*-cuprate) single crystal which contains two different insulating blocks in the unit cell in-between the CuO conducting/superconducting planes. These blocks form two different Josephson junctions between the CuO planes in the superconducting state, for the polarization when the electric field of the external radiation is directed perpendicular to the CuO planes (along the c crystallographic axis). Such a system was predicted to show a specific excitation – the transverse Josephson plasmon [5]. With the help of the BWO technique we have found this excitation; it is seen as a peak in the conductivity spectrum (transverse response), lying between the two *longitudinal* plasmon excitations displayed in the loss-function spectra (longitudinal response), see Fig.7 [6].

6. THz-subTHz response of a gas: water vapor

Water exists in two forms of *ortho-* and *para*-isomers, according to the relative arrangement of hydrogen spins in the H_2O molecule. In Nature the two modifications at room temperatures are in an equilibrium *ortho:para* = 3:1 state. Study of these water isomers is of great importance in any sense since water is the basis of life on the Earth. We managed to violate the natural 3:1 equilibrium and to detect the relative *ortho-para* content by using the THz-spectroscopic technique and detecting the intensities of specific rotational absorptions [7]. The illustration is shown in Fig.8.

7. THz-subTHz magnetic spectroscopy

The real and the imaginary part of the magnetic permeability are directly determined by measuring Tr(ν) and f (ν) spectra [1,8]. Due to the fact that in many cases the magnon excitations are relatively narrow, measurement of the magnetic permeability is essentially simplified, as illustrated in Fig.9: first the $\varepsilon'(\nu)$, $\varepsilon''(\nu)$ spectra are measured outside of the magnetic dispersion range and the obtained vales are extrapolated into it (dashed lines); after that the $\mu'(\nu)$, $\mu''(\nu)$ spectra are calculated from Tr(ν) and f (ν) spectra. The example of Fig.9 shows the magneto-dipole transitions within the ground state multiplet of a molecular magnetic cluster Mn12*ac* [8].

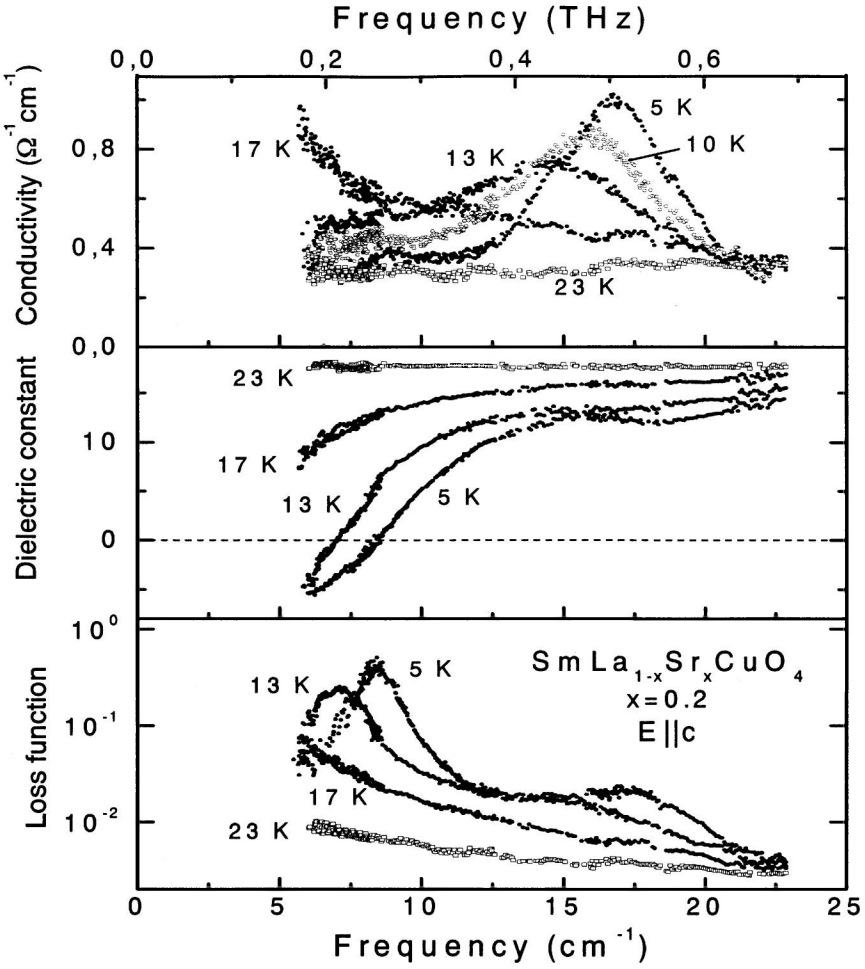

Fig.7. Directly measured subTHz spectra of dynamic conductivity, dielectric constant and loss function for Sm-LSCO single crystal. In the normal state the spectra are Drude-like. In the superconducting state two longitudinal Josephson plasmons develop in the loss function spectrum and a new type of excitation, the transverse Josephson plasmon, in the conductivity spectrum [5,6].

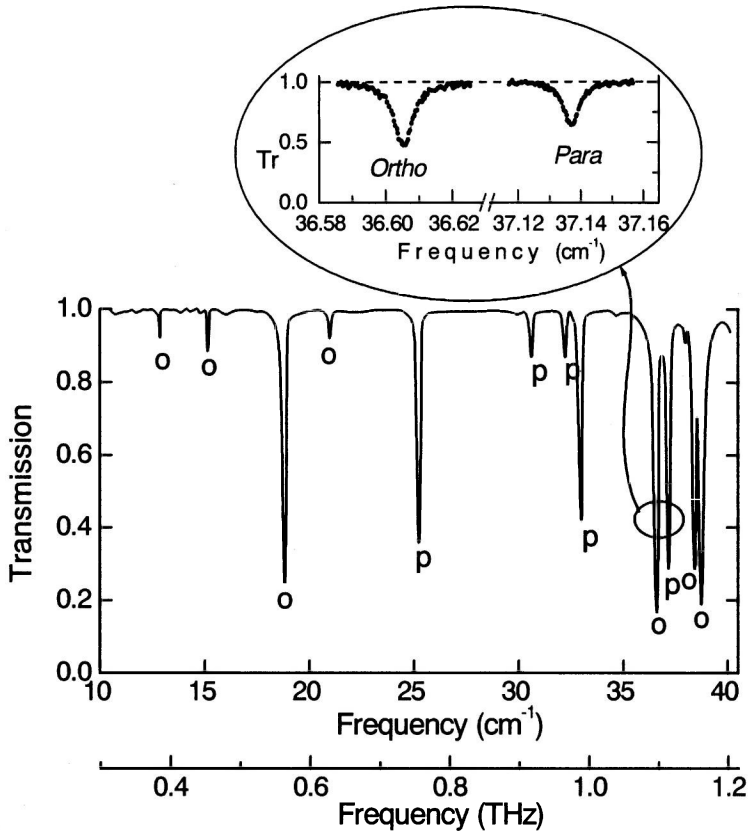

Fig.8. Transmission spectra of the H_2O vapor. "O" and "p" mark rotational absorption lines corresponding to *ortho-* and *para*-isomers, respectively. A doublet of closely located lines used for detecting the *ortho/para* ratio is shown in details in the inset [7].

8. THz-subTHz reflectivity

When needed, the reflection coefficient R is complementary measured in a quasioptical arrangement in conditions of normal incidence [1]. This happens when the sample is too highly absorbing (or conducting), so that it is not

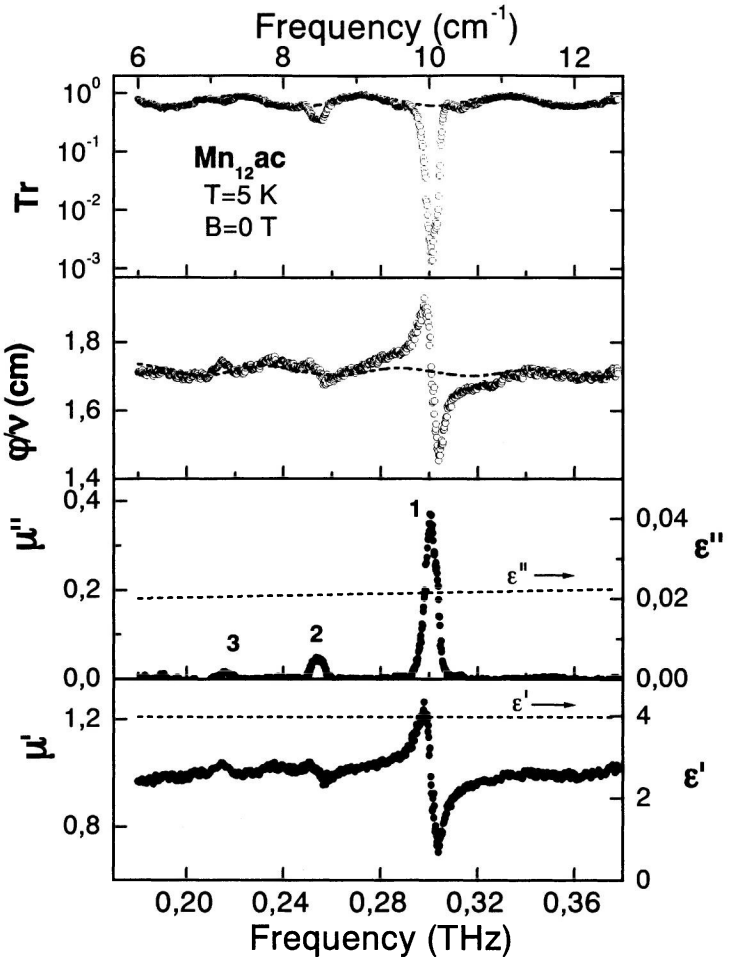

Fig.9. Spectra of real and imaginary parts of the magnetic permeability of a molecular magnet $Mn_{12}ac$, determined basing on the transmission and phase spectra; dashed lines show dielectric parameters of the sample (see text). Three magneto-dipole transitions are clearly seen corresponding to transitions within the ground state multiplet [9].

possible to prepare thin enough layer to measure its transmission characteristics, for example, in the case of highly conducting or superconducting materials.

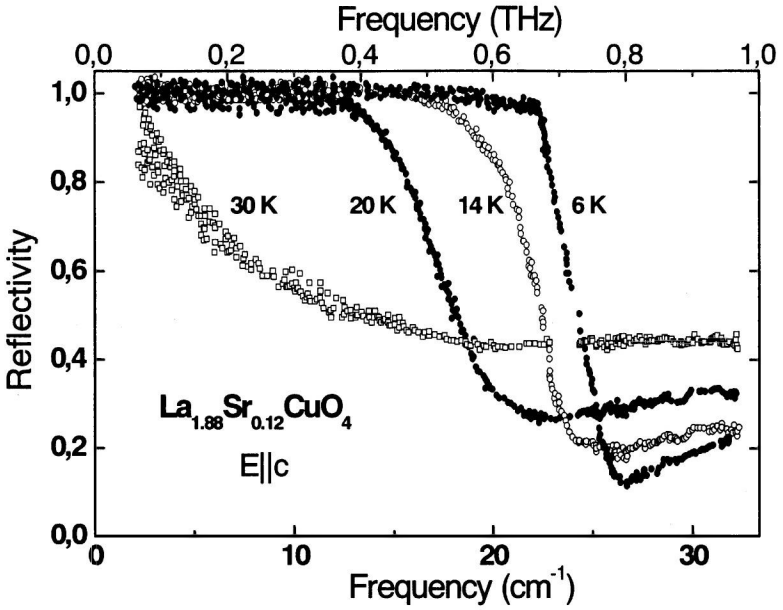

Fig. 10. SubTerahertz spectra of reflectivity of LSCO crystal for polarization across the CuO superconducting planes, E||c. In the normal state the spectrum displays the Hagen-Rubens regime of a poor metal. In the superconducting state a plasma edge develops due to the longitudinal plasma excitation of the Cooper pairs condensate.

Appropriately designed sample holders and cryostats allow absolute accuracy of reflection coefficients measurements of better than ± 0.5% at the level of R close to 99% - 100%. Variety of dielectric, conducting and superconducting materials has been measured; an example on the High-T_c LSCO crystal is depicted in Fig.10, which shows a plasma edge coming from collective dynamics of the Cooper pairs condensate in the superconducting state.

9. THz-subTHz spectroscopy of thin films

The BWO-spectroscopic technique can successfully be used for measurements of THz-subTHz response of thin films on a substrate. First, the dielectric properties of a substrate (not coated with the film) are determined in a standard way and then the transmission and the phase shift of the two-layered system – the film on a substrate – are measured. After that the dielectric parameters of the film are directly calculated from Tr(ν) and f(ν) using

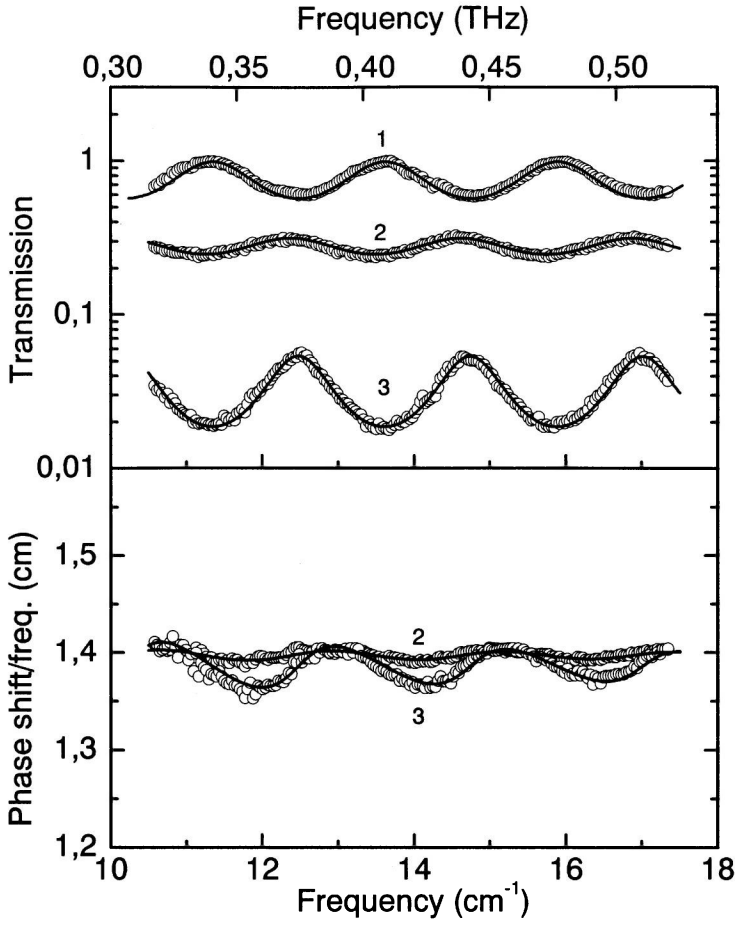

Fig.11. SubTerahertz spectra of transmissivity and phase shift of a quartz substrate (1) and of two diamond-like films (2 and 3) of different thickness on the quartz substrate. Dots are experiment and lines – fit, obtained with the Fresnel formulas allowing for determination of the subTHz properties of the films and of the quartz substrate [10]. Maxima are due to interference within the substrate. The p-shift of the maxima/minima for the coated substrates are due to the change of the phase on the interface "quartz-film" [11].

corresponding Fresnel expressions for a two-layered system. An example of such measurement is shown in Fig.11. The spectra in this figure correspond to a new class of coatings which are very promising for applications – the diamond-like films; dots represent experimental data and the lines show the fit from which dielectric parameters of the films and of the substrate were determined [10].

10. THz-subTHz spectroscopy of magnetic excitations in solids: $La_{1-x}Sr_xMnO_3$ manganites

Resonance frequencies of many kinds of magnetic excitations in solids lie in the THz-subTHz range. In this paragraph we present recent results of the study of various magnetic excitations in two classes of magnets: colossal magnetoresistance (CMR) manganites $La_{1-x}Sr_xMnO_3$ ($0 \le x \le 0.175$) and single-

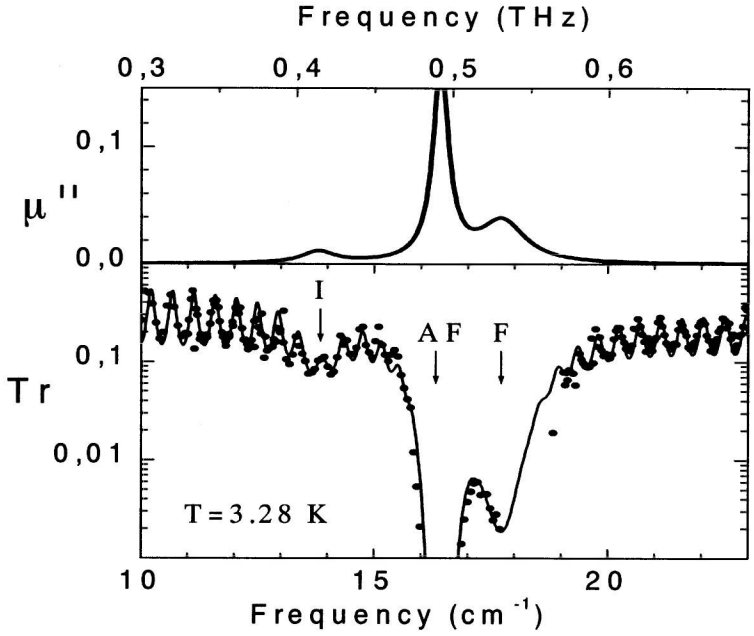

Fig.12. Transmission Tr(ν) spectra of $La_{0.99}Sr_{0.01}MnO_3$ single crystallite plate (lower panel) and extracted spectra of imaginary part of permeability (upper panel). Symbols – experiment, lines – fit by Fresnel's formulae for plane parallel layer and three Lorentzian modes (F, AF, I) in the complex permeability $\mu^*(\nu)$. Oscillations in Tr(ν) outside the lines are due to interference.

molecule based magnet (cluster) $Mn_{12}ac$.

One of the basic features of the CMR manganites is a transformation of their magnetic structure from an antiferromagnetic and insulating state at x=0 into a ferromagnetic and metallic one with increasing of concentration of divalent Sr ions up to x~0.17-0.3 [12]. Study of magnetic excitations is sensitive to the magnetic structure and offers a good possibility to investigate its evolution with the Sr doping and to clarify one of the most controversial problem concerning an elucidation whether the transformation of the magnetic structure occurs via a canted phase [13] or a phase separation into antiferromagnetic insulating and ferromagnetic metallic domains [14].

Two closely spaced antiferromagnetic resonance (AFMR) modes in the pure $LaMnO_3$, quasiferromagnetic (F) and quasiantiferromagnetic (AF) (respectively, at 18.1 and 17.3 cm^{-1} at 4.2 K) evolve dramatically with increasing the Sr (hole) concentration [15]. For x~1% an additional weak impurity (I) mode was observed in the transmission spectra below the main AFMR F and AF modes (Fig.12), which could indicate on magnetic inhomogeneities, in particular, on an existence of regions with larger magnetization (canting) due to double exchange in the vicinity of holes localized at Mn ions.

For higher Sr concentrations the F mode at ~17 cm^{-1} disappears while the low frequency (impurity) mode remains and shifts to smaller frequencies. Its excitation condition ($h \perp c \| m$, where m is a spontaneous magnetization) corresponds to the F-mode symmetry that allows to identify it with the latter and to conclude on the transformation of the I mode into the F one. The AF mode frequency is only slightly shifted to smaller values. An external magnetic field B affects significantly the mode's positions which reveal a strong dependence on an orientation B with respect to the crystallographic axes (Fig.13). Such a behavior of frequencies, including also the effect of the magnetic field, is consistent with a canted (and probably modulated) magnetic structure [15-17]. For $0.1<x<0.15$ (ferromagnetic insulator state) complicated electron spin resonance (ESR) in transmittivity spectra was observed in magnetic fields for a Faraday geometry both in the field sweep and frequency sweep runs, which can be well explained by a single ferromagnetic resonance (FMR) mode and taking electrodynamic interference effects into account [17]; no AFMR modes were found for these concentration range.

A further increasing of x ($x \geq 0.15$) results in a ferromagnetic and conducting states in $La_{1-x}Sr_xMnO_3$ which was studied by reflectivity R measurements. An example of field-sweep ESR spectra dR/dH is shown in Fig.14 for $La_{0.825}Sr_{0.175}MnO_3$. In addition to the intensive FMR line, a weak line of the ferromagnetic antiresonance (FMAR) was also observed at lower fields corresponding to the $\mu'(B) = 0$ [17]. The spectra dR/dH are nicely described by Fresnel's formulae. The intensity of both lines decreases for decreasing

temperature. This effect is easily explained as being due to increasing of the conductivity; its value $\sigma \sim 10^4\ \Omega^{-1}cm^{-1}$ estimated at low temperature is in agreement with the dc resistivity data.

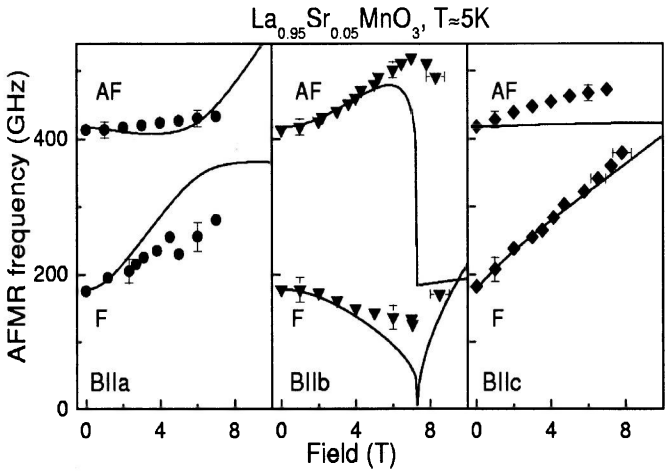

Fig.13. Magnetic field-dependence of the resonance frequencies of the AFMR lines in $La_{0.95}Sr_{0.05}MnO_3$ at low temperatures. Dots - experiment, lines - theory for the canted magnetic structure [16].

The evolution of the found spin gaps, i.e., quasiferromagnetic and quasiantiferromagnetic modes as well as impurity one, with increasing of the Sr concentration displays a strong softening of the quasiferromagnetic mode which occurs via the appearance of the low-lying impurity mode for small concentration range $x<0.02$ and its subsequent transformation to the main branch of the F mode while the upper F-mode branch dies at $x>0.02$. The spin gap of the AF mode is only slightly shifted to smaller values.

In the whole, our study of the magnetic excitation in $La_{1-x}Sr_xMnO_3$ reveals that its magnetic structure is transformed, with increasing x, from antiferromagnetic to the canted modulated states ($x<0.1$) characterizing a significant inhomogeneity for $x\sim1\%$ and then - to ferromagnetic insulator ($0.1<x<0.15$) and ferromagnetic metallic ($x\geq0.15$) states.

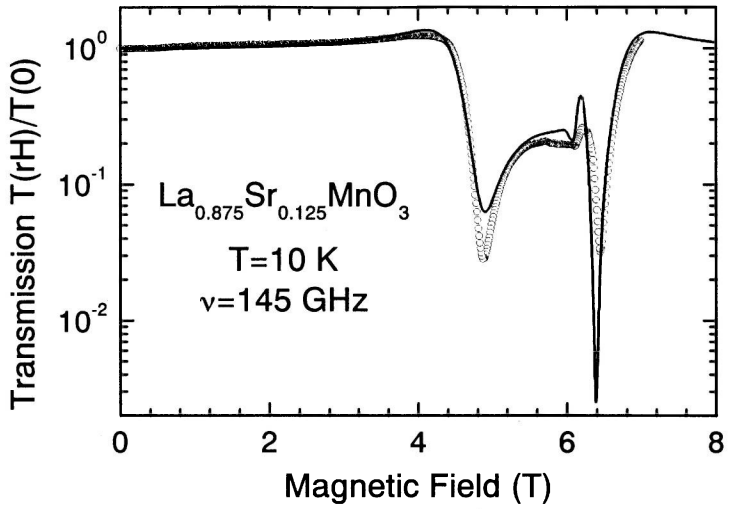

Fig.14. ESR spectra of $La_{0.875}Sr_{0.275}MnO_3$ in the Faraday reflection geometry. Line splitting of the FMR mode is due to anisotropy of the crystal field below the structural hombohedral-to-orthorhombic transition. Dots – experiment, line – theory.

11. THz-subTHz spectroscopy of magnetic excitations in solids: Mn12*ac* molecular magnet

Mn_{12}*ac* is a prime example of single-molecule magnet exhibiting mesoscopic quantum phenomena like quantum tunneling of magnetization [18]. The key role in these phenomena is played by the crystal field (CF) splitting of the ground S = 10 multiplet of exchange-coupled manganese ions. The CF splitting and corresponding magnetodipolar transitions between low-lying CF states were clearly observed in the transmission (Fig.15) and permeability (Fig.9) spectra [9,19,20]. The intensity of the transitions is changed significantly with the temperature lowering due to the variation of the CF states population. The lineshape of the observed transitions is Gaussian with a linewidth practically independent on the temperature, its origin is determined by a random distribution of the CF due to local defects in a crystal and random distributions of the internal magnetodipolar and hyperfine fields. At high frequencies (ν>33 cm^{-1}) a wide band was observed in transmission spectra which could be related to the transitions to the excited multiplet S=9. However, for the radiation with

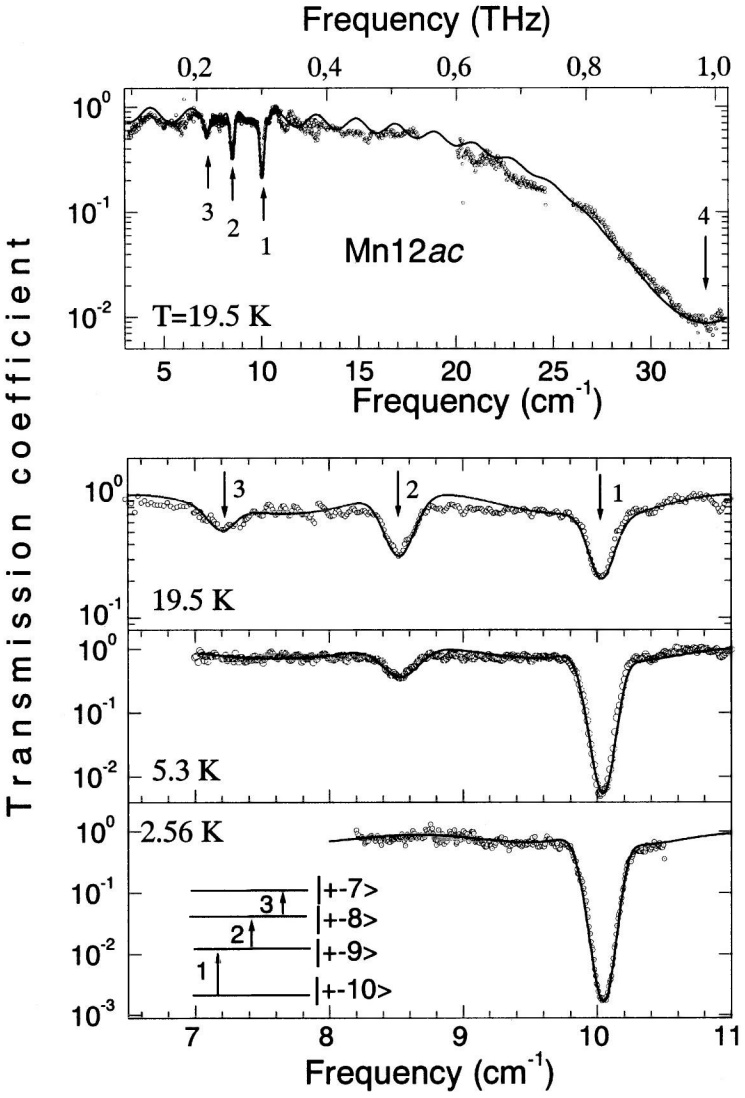

Fig.15. Transmission spectra of a plane-parallel Mn_{12}-ac pellet in a wide frequency range (upper panel) and near the CF transitions (inset in lower panel). Dots - experiment, lines – theory (Gaussian lineshape).

q=0 this transitions are expected to be forbidden on a spin quantum number and the origin of a permission is not clear yet.

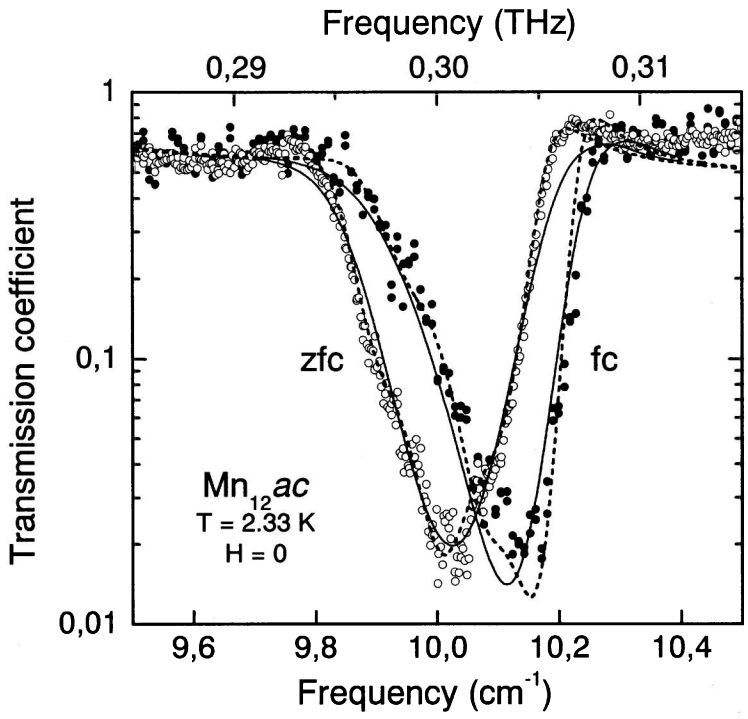

Fig.16. Transmission spectra of a plane-parallel $Mn_{12}ac$ crystalline mosaic sample near the $|\pm10\rangle \rightarrow |\pm9\rangle$ CF transitions, measured in zero magnetic field in the zero-field-cooled (zfc) and field-cooled (fc) states. Dots are experiment, lines – theory [21].

Using the oriented single crystalline mosaic of $Mn_{12}ac$ with easy (C_4) axis parallel to the sample plane, we have observed that the lineshape of CF transitions $|\pm10\rangle \rightarrow |\pm9\rangle$ is determined by the magnetic history [21]. The absorption lines are symmetric and Gaussian for the non-magnetized state obtained by zero-field cooling (zfc) (Fig.16). In the magnetized state which is reached when the sample is cooled in a magnetic field (fc), however, they are asymmetric and are shifted up by 0.1 cm^{-1} even in the absence of an external magnetic field. These observations are quantitatively explained by inhomogeneous symmetrical (Gaussian) broadening of the CF transitions

combined with a contribution of off-diagonal components of the magnetic susceptibility to the effective permeability $\mu_{eff}(\nu) = \mu_{xx}^2 - \mu_{xy}\mu_{yx} / \mu_{yy}^2$. This can be qualitatively understood as a redistribution of the interacting modes superposed in the total inhomogeneously broadened line which dynamically occurs via the magnetic medium, i.e., via different components of its susceptibility depending on the magnetic state [21].

References

[1] Kozlov G.V., Volkov A.A. Coherent Source Submillimeter Wave Spectroscopy. Topics in Applied Physics, **74**, p.51, ed. G.Gruner, (Springer-Verlag, 1998).

[2] M.Born, E.Wolf. Principles of Optics, 6th ed. (Cambridge University Press, Cambridge 1999).

[3] A.Schwartz et al. Resonant techniques for studying the complex electrodynamic response of conducting solids in the millimeter and submillimeter wave spectral range. Rev. Sci. Instrum., **66**, 2943 (1995).

[4] S.Mair et al. Spatial and spectral behavior of the optical near field studied by a terahertz near-field spectrometer. Appl. Phys. Lett. **84**, 1219 (2004).

[5] D. Van der Marel, A.Tsvetkov. Transverse optical plasmons in ordered and disordered Josephson-coupled superconducting multilayers. Czech. J. Phys. **46**, 3165 (1996).

[6] T.Kakeshita et al. Transverse Josephson plasma mode in T* cuprate superconductors. Phys. Rev. Lett. **86**, 4140 (2001).

[7] V.Tikhonov, A.Volkov. Separation of water into its ortho and para isomers. Science **296**, 2363 (2002).

[8] A.Balbashov et al. Submillimeter spectroscopy of antiferromagnetic dielectrics: Rare-earth orthoferrites. In "High Frequency Processes in Magnetic Materials", ed. G.Srinivasan, A.Slavin (World Scientific, Singapore 1995); J.van Slageren et al. Frequency-domain magnetic resonance spectroscopy of molecular magnetic materials. Phys. Chem. Chem. Phys. **5**, 3837 (2003).

[9] M.Dressel et al. Direct Observation of Quantum Tunneling and Relaxation in Mn_{12}ac. Phys. Rev. B **67**, 060405 (2003).

[10] O.Ryabova et al. Unpublished.

[11] B.Gorshunov et al. Measurement of electrodynamic parameters of superconducting films in far-infrared and submillimeter frequency ranges. Int. J. IRMMW **14,** 683 (1993).

[12] E.O.Wollan and W.C.Koehler, Neutron diffraction study of the magnetic properties of the series of perovskite-type compounds [(1-x)La, xCa]Mno_3. Phys.Rev., **100**, 545 (1955).

[13] P.-G. de Gennes, Effects of double exchange in magnetic crystals. Phys. Rev., **118**, 141 (1960)

[14] E. Dagotto, et al., Colossal magnetoresistant materials: The key role of phase separation. Phys. Rep., **344**, 1 (2001).

[15] A.A.Mukhin, et al., Antiferromagnetic resonsnce in the canted phase of $La_{1-x}Ca_xMnO_3$: experimental evidence against electronic phase separation. Europhys. Lett., **49** , 514 (2000).

[16] A.Pimenov, et al., High-field antiferromagnetic resonance in single-crystalline $La_{0.95}Sr_{0.05}MnO_3$: Experimental evidence for the existence of a canted magnetic structure. Phys. Rev.B, **62**, 5685 (2000).

[17] D.Ivannikov, et al., High-field ESR spectroscopy of the spin dynamics in $La_{1-x}Ca_xMnO_3$ ($x<0.175$). Phys. Rev. B, **65**, 214422 (2002).

[18] J.R.Friedman et al., Macroscopic measurements of resonant magnetization tunneling in high-spin molecules. Phys. Rev. Lett. **76**, 3830 (1996)

[19] A.A.Mukhin, et al., Submillimeter spectroscopy of Mn_{12} magnetic cluster. Europhys. Lett,. **44**, 778 (1998).

[20] A.A.Mukhin, et al., Submillimeter spectroscopy of electronic transitions and macroscopic quantum tunneling of magnetization in molecular nanocluster. Physics – Uspekhi , **34**, 1306 (2002).

[21] S.Vontragool et al., Asymmetric lineshape due to inhomogeneous broadening of the crystal-field transitions in Mn_{12} acetate single crystals. Phys. Rev. B, **69**, 104410 (2004).